Study of magnetic materials using helicity-modulated X-ray magnetic circular dichroism

H. Maruyama

Department of Physics, Faculty of Science, Okayama University, 3-1-1 Tsushima-Naka, Okayama, Okayama 700-8530, Japan. E-mail: maruyama@mag.okayama-u.ac.jp

A new helicity-modulation technique has been applied for recording X-ray magnetic circular dichroism (XMCD) at the *K*-absorption edge in transition-metal magnetic materials. This technique enables the measurement of the XMCD spectrum with high precision and under extreme conditions. The refined spectrum is presented at the Fe *K* edge for pure Fe, Fe_4N and Co-ferrite. The method is very promising for site-assignment of magnetic cations and for detailed investigation of the magnetic states in a local environment. In Mn_3MC perovskites, the dependence of the Mn *K*-edge XMCD spectrum on temperature and magnetic field demonstrates that the orbital moments are closely associated with the magnetic phase transition. New information obtained from the refined spectrum and novel phenomena observed in temperature and field variations is presented.

Keywords: X-ray magnetic circular dichroism; helicity-modulation method; iron compounds; Mn_3MC perovskites; magnetic phase transition.

1. Introduction

Polarization properties have been extensively investigated at the third-generation synchrotron radiation sources. In particular, circular polarization is essential in studying the magnetic properties of various magnetic materials. X-ray magnetic circular dichroism (XMCD) has been widely used for characterizing electronic and magnetic states since the dichroism was first observed at the Fe *K* edge of pure iron. Our group has recently developed a new helicity-modulation technique using a synthetic diamond crystal and hard X-rays. The helicity-modulation technique enables us to obtain more precise XMCD spectra and to perform experiments under extreme conditions. In this paper, several applications for studying electronic and magnetic properties are presented.

At the first stage of the XMCD study, a bending magnet was employed in inclined geometry to incorporate the circularly polarized photons (Schütz *et al.*, 1987). Then, highly polarized intensive X-rays, generated by an elliptical multipole-wiggler (Maruyama *et al.*, 1991) or a helical undulator (Goulon *et al.*, 1995), were developed to record XMCD spectra. The use of a quarter-wave plate was originally proposed by Ishikawa *et al.* (1992) as an X-ray optical device to produce the circularly polarized X-rays, and the phase plate was combined with an energy-dispersive technique for XMCD measurements (Giles *et al.*, 1994). Furthermore, the phase plate has been applied to fast helicity reversal, establishing the helicity modulation at SPring-8 BL39XU (Suzuki *et al.*, 1998). Remarkable improvements in XMCD spectra have demonstrated the efficiency of this method (Suzuki *et al.*, 1999). A new hybrid helical undulator has also realised helicity modulation using an X-ray source (Rogalev *et al.*, 1999). Since the helicity modulation does not require reversal of the magnetic field applied to the sample, it should be very practical and applicable for various experiments. Using the helicity-modulation method, studies in materials science will be extended by improved XMCD measurements.

2. XMCD in helicity-modulation mode

For recording an XMCD spectrum, two methods have been commonly used: magnetic field reversal and helicity reversal. In the hard X-ray region, an XMCD spectrum is generally weak, typically less than 10^{-3} of the edge-jump in X-ray absorption near-edge structure (XANES) at the *K* edge. Furthermore, the spectrum usually shows a complicated profile, *e.g.* the spectrum at the *L* edges of rare-earth elements. Consequently, a long-term data accumulation is required to record a reliable spectrum, thus restricting a systematic experiment. With the field-reversal method, relatively low fields are available for limited magnetic saturation and the field reversal gives rise to noise caused by sample vibration. The helicity-reversal mode overcomes these limitations and is preferred to the conventional field-reversal mode.

Polarization tunability has been demonstrated using a diamond phase plate in combination with a linear undulator (Maruyama *et al.*, 1999). At SPring-8 BL39XU, four diamond crystals, of 0.3–0.7 mm in thickness, cover the energy range from 5.7 to about 14 keV. An extension below 5 keV is restricted because of the difficulty in fabricating thinner diamond crystals and the serious absorption of the phase plate. The phase plate is capable of fast helicity reversal with an almost 100% degree of circular polarization (P_C). The helicity-modulation system mainly consists of a phase retarder assembly and a lock-in amplification of dichroic signal converted through a logarithmic circuit. The offset angle of the phase plate is regulated according to the photon energy, the thickness of diamond crystal and the reflection index. For example, using a diamond of 0.57 mm thickness at the Fe *K* edge, when the offset angle was adjusted to about ± 130 arcsec from the Bragg condition with the 220 reflection in the Laue geometry, a circular polarization of $|P_C| = 0.998$ was attainable and the modulation frequency was optimized at $f = 40$ Hz. Applicable frequency ranges were up to 200 Hz. Furthermore, the dichroic measurement has been successfully extended over a very wide energy range (magnetic EXAFS) by synchronizing the undulator gap, the Bragg angle of monochromator and the offset angle of phase plate. A more detailed technical description has been given elsewhere (Suzuki *et al.*, 1998, 1999).

3. Performance of the helicity-modulation method

As a typical example, Fig. 1 shows the XMCD and XANES spectra recorded by the helicity-modulation method at the Fe *K* edge in Fe metal, Fe_4N and Co-ferrite ($CoFe_2O_4$). The XMCD spectrum shows the following improvements compared with the previous data: (i) the signal-to-noise (S/N) ratio is improved significantly and the noise level is reduced to about 5×10^{-4}; (ii) the dichroic signal detection efficiency, defined as the XMCD/XANES ratio, is improved by an order of magnitude; (iii) a high statistical accuracy is obtained because the data accumulation time has been shortened by an order of magnitude. These improvements are the result of the combination of the following features: the low-emittance and brilliant light source, a high polarization, the modulation technique acting as a low-pass filter, and the magnetic field non-reversal being effective for noise elimination. Above all, the synthesis of a diamond single crystal with high quality (Sumiya *et al.*, 1997) is crucial in order to realise these achievements. These advantages have led to improved performance. First, fine structures are observable. Second, weak and additional dichroic effects are detectable. Third, measurements under extreme

conditions, *e.g.* high magnetic field, high pressure, low temperatures, *etc*., can be extended for studying magnetic states. Finally, systematic measurement can be made easily.

4. XMCD studies extended by the helicity-modulation method

The aforementioned advantages have been applied for studying magnetic properties. Newly derived information from the improved spectra is presented regarding site selectivity, angular momentum sensitivity and element specificity.

4.1. *Site selectivity*

An accurate XMCD spectrum is crucial for recording fine structures and/or weak signals. The Fe *K*-edge XMCD and XANES of pure Fe, Fe_4N and Co-ferrite are shown in Fig. 1. These materials are categorized as metal (Fe), metallic compound (Fe_4N) and insulator (Co-ferrite). Chemical shift follows this order; in particular; ferrite is characterized by the pre-peak structure. In the XMCD spectrum, Fe_4N perovskite shows a positive and sharp peak at the edge (Fig. 1*b*). This structure has never been detected by the conventional method. Although the origin of this structure has not been identified yet, it should be explained in terms of the covalency. This point may be a good criterion of a theoretical calculation. The overall profile is well reproduced by a multiple-scattering calculation considering two Fe sites (Nagamatsu *et al.*, 2000). Fe ions occupy the face-centred site Fe(*f*) and the cubic corner site Fe(*c*). Magnetic states in Fe(*c*) ions are similar to those in pure Fe, which is metallic. On the other hand, those in Fe(*f*) ions are strongly affected by the neighbouring N anion and eventually have covalent character as a result of charge transfer.

The Fe *K*-edge XMCD of the Fe oxides, garnet or spinel-type ferrite, could be roughly interpreted as a superposition of pre-peak structure arising from Fe(T_d) ions in tetrahedral (T_d) sites and the main peak mainly resulting from Fe(O_h) ions in octahedral (O_h) sites (Kawamura *et al.*, 1997). A dispersion-type XMCD spectrum in ferrites has been successfully reproduced by calculations based on the atomic model taking into account the *p*–*d* hybridization and spin-orbit interaction (Harada & Kotani, 1994). One can consider, therefore, that the Fe *K*-edge XMCD in Co-ferrite (see Fig. 1*c*) is ideally composed of the contributions of $Fe^{3+}(T_d)$ and $Fe^{3+}(O_h)$ ions

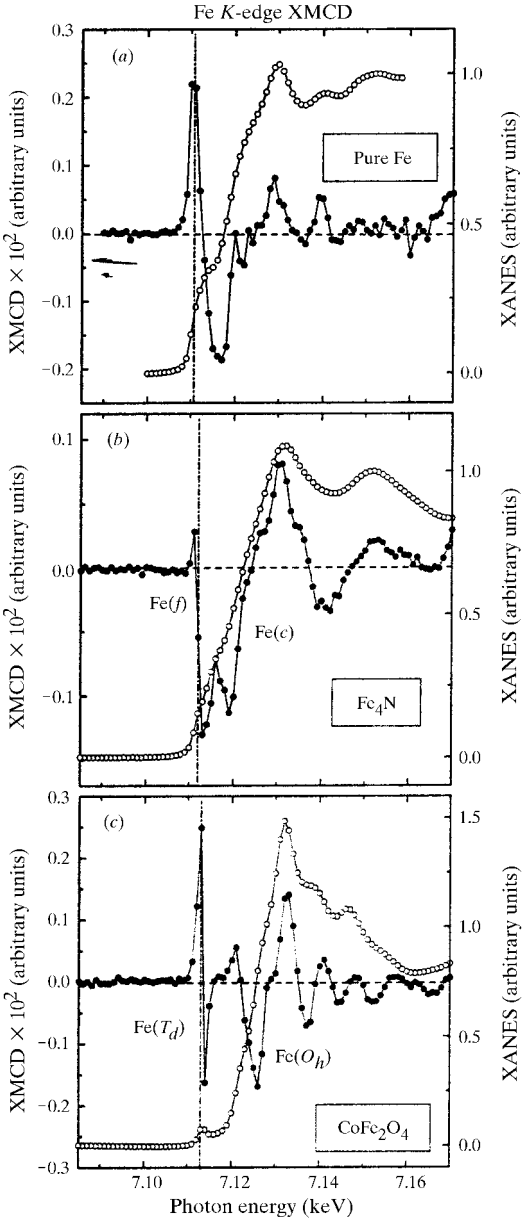

Figure 1
XMCD and XANES spectra at the Fe *K* edge for (*a*) pure Fe, (*b*) Fe_4N, and (*c*) $CoFe_2O_4$.

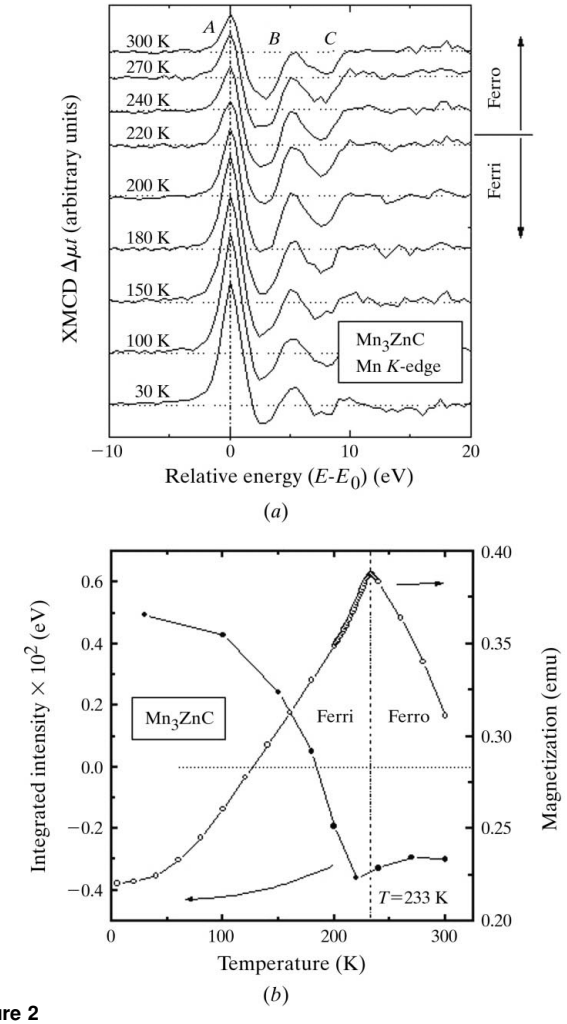

Figure 2
Temperature variation of (*a*) the Mn *K*-edge XMCD spectrum of Mn_3ZnC under H = 0.6 T, and (*b*) the integrated intensity, in comparison with the variation of magnetization.

resulting from the substitution of Co^{2+} by $Fe^{2+}(O_h)$. This has been verified by the *K*-edge XMCD spectrum for the substituted Mn, Co, Ni or Cu cations, in which the contribution appears in the main-peak region in inverse spinel Co-, Ni- or Cu-ferrite, whereas it is distributed in both the pre-peak and the main-peak regions in normal spinel Mn-ferrite. It could be possible to make site assignment using the precise XMCD spectrum, which is an informative tool for studying magnetic ions in a local environment as well as for Mössbauer spectroscopy.

4.2. *Angular-momentum sensitivity*

The case of Mn_3MC (M = Zn and Ga) perovskites, which have attracted interest because of a variety of magnetic phase transitions, is presented. Fig. 2(*a*) demonstrates the temperature variation of the spectrum of Mn_3ZnC (Uemoto *et al.*, 2001). In the ferromagnetic phase, the spectrum shows a dispersion-type profile having a positive peak just on the edge (labelled as *A*) and two negative peaks (labelled as *B* and *C*) at $(E - E_0) \simeq 2.5$ and 7 eV. Below the transition temperature (T_t = 233 K), the positive peak increases with decreasing temperature, although the magnetization decreases. On the other hand, the negative peaks normally show a decrease in intensity as well as a change in magnetization as a result of the second-order transition (Fruchart & Bertaut, 1978). It is shown obviously in Fig. 2(*b*) that the integrated intensity first maintains a negative sign in the ferromagnetic phase and then starts to decrease near T_t. It then changes sign from negative to positive at about 180 K.

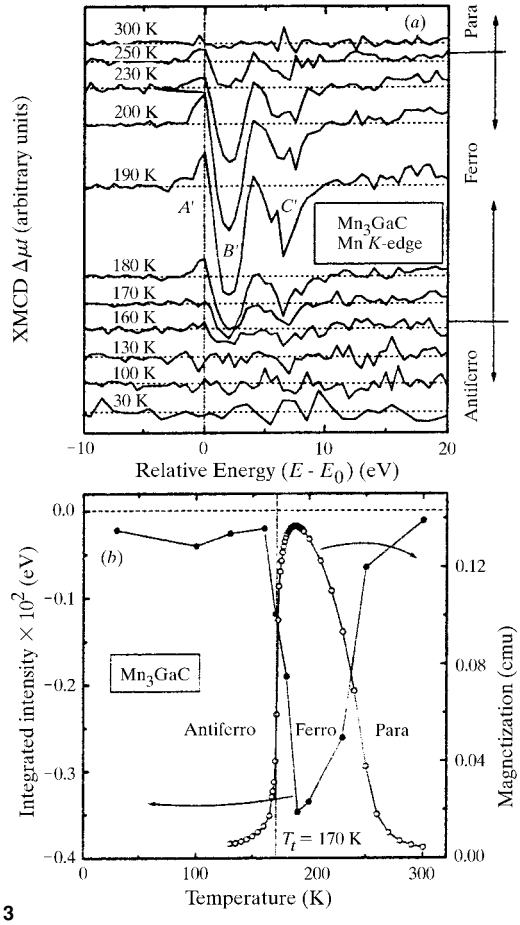

Figure 3
Temperature variation of (*a*) the Mn *K*-edge XMCD spectrum of Mn_3GaC under H = 0.6 T, and (*b*) the integrated intensity, in comparison with the variation of magnetization.

The XMCD spectrum ($\Delta\mu t$) may be described phenomenologically as

$$\int(\Delta\mu t)\,\mathrm{d}\omega \propto P_C\, M(T, H)\cos\theta\,(\Delta\rho/\rho), \qquad (1)$$

where $M(T, H)$ is the magnetization as a function of T and H, θ is the angle between the magnetic moment and the incident X-ray wavevector, ρ is the total density-of-states, and $\Delta\rho$ is the magnetic polarization. The present result is not in agreement with the general understanding and this is the first observation of such a drastic change in the XMCD spectrum. How can we explain this peculiarity? According to the magneto-optical sum rule for the *K* edge (Igarashi & Hirai, 1994), the integrated intensity is related to the expectation value of orbital angular momentum per Mn 4*p* hole. Hence, the present data indicate that the orbital moment in the *p* unoccupied states is not quenched and changes sign from positive to negative following the phase transition. This means that the Mn *p* conduction bands have the orbital moments antiparallel to the 3*d* moments below 180 K. It is generally accepted that the *K*-edge XMCD originates in the 3*d*–4*p* hybridization *via* neighbouring atoms and the spin-orbit coupling. Therefore, the observed behaviour could be associated with the canted-ferromagnetic structure of Mn_3ZnC in the ferrimagnetic phase.

4.3. *Angular momentum under high magnetic fields*

Isomorphic Mn_3GaC perovskite shows a first-order transition from ferromagnetism to antiferromagnetism (T_t = 170 K) (Fruchart & Bertaut, 1978; Kaneko *et al.*, 1987). Fig. 3(*a*) shows the temperature variation of the XMCD spectrum of Mn_3GaC (Uemoto *et al.*, 2001). The intensity of the positive peak at the edge (labelled as *A*′) was drastically reduced in comparison with Mn_3ZnC. The spectrum is characterized by two negative peaks (labelled as *B*′ and *C*′) at $(E - E_0) \simeq 2$ and 6.5 eV, which are observed only in the ferromagnetic phase ranging from 170 K to T_c = 260 K. The temperature dependence of the intensity is in good agreement with that of magnetization, as shown in Fig. 3(*b*). The sum rule implies that Mn ions possess positive orbital moments. Even if Mn_3GaC is in an antiferromagnetic ground-state below T_t, ferromagnetism can be induced under high fields; this is metamagnetic transition. In Mn_3GaC, the metamagnetism is observed in the range 130–170 K under 10 T. To investigate the Mn magnetic states under a high magnetic field, a split-type superconducting magnet was used for the experiment up to 10 T at low temperatures.

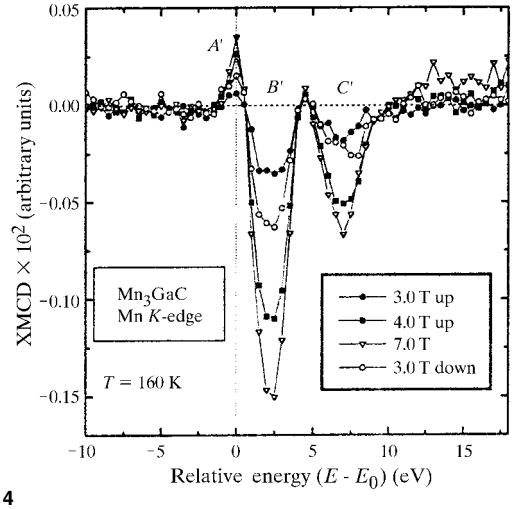

Figure 4
Magnetic field variation of the Mn *K*-edge XMCD of Mn_3GaC up to 7 T at T = 160 K.

Fig. 4 shows the field variation of the XMCD spectrum of Mn_3GaC at T = 160 K, below T_t. The intensity increases significantly with the applied field, while no change is observed in the profile. The integrated intensity closely follows the magnetization curve together with the hysteresis phenomenon, as shown in Fig. 5. It should be noted that the intensity maintains a negative sign, which means that the orbital moments are always positive. It is considered that the spectrum reflects the ferromagnetic component of the spin-flip structure under high field. The spin-flip state in Mn_3GaC is clearly different from the canted-ferromagnetic state in Mn_3ZnC. The difference in Mn magnetic states may be ascribed to a modification in electronic structure induced by the second metal, Ga or Zn. The non-collinear spin structure is strongly related to the magneto-anisotropy through the spin-orbit coupling. These features in Mn_3MC perovskites, observed for the first time, indicate that the orbital moments are associated with the magnetic phase transition.

4.4. *Element specificity*

The helicity-modulation method is capable of recording magnetic hysteresis in a dichroic signal. Since an XMCD spectrum has element specificity, the dichroism in helicity-modulation mode enables the monitoring of the element-specific magnetizing process in hard magnetic materials and the recording of the field-cooling process in spin-glass materials. This type of measurement is rather difficult using the magnetic-field-reversal method. XMCD in helicity-modulation mode functions as an element-specific magnetometry by monitoring the dichroic signal when the photon energy is tuned to a value taking the maximum intensity. In a Gd/Fe multilayer, hysteresis loops have been measured separately for each constituent (Koizumi *et al.*, 2000).

4.5. *Application to miscellaneous experiments*

The helicity-modulation method is a general technique that can be applied in many other experiments in order to extract the magnetic effect. For example, in resonant inelastic X-ray scattering (RIXS), the superimposed MCD effect is useful for a fuller understanding of electronic states associated with the X-ray absorption (Krisch *et al.*, 1996). MCD-RIXS using the helicity-modulation method will be a powerful tool for studying the polarization or angular effect on magnetic states.

For recording natural dichroism (Alagna *et al.*, 1998), the helicity-modulation method is ideal because there is no requirement for field-direction reversal. Electronic states in non-magnetic or chiral materials are also intriguing subjects.

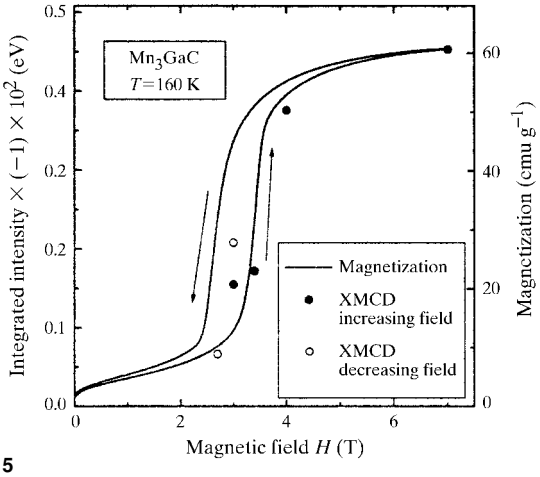

Figure 5
Integrated intensity of the Mn *K*-edge XMCD of Mn_3GaC as a function of magnetic field, following the metamagnetic phase transition, in comparison with the magnetization curve at T = 160 K.

5. Concluding remarks

The helicity-modulation technique has been found to improve XMCD spectra with regard to the signal-to-noise ratio, the efficiency and the statistical accuracy. The refined spectra enable site-assignment of magnetic cations and a detailed study of magnetic states, which is useful in understanding magnetic properties, magnetic structures and magnetizing processes. Furthermore, systematic measurements are easily carried out. XMCD experiments under extreme conditions are now possible for studying magnetic phase transitions caused by temperature, a magnetic field or pressure. For the first time, it has been observed that the orbital moments are closely associated with the magnetic phase transition in Mn_3MC perovskites. However, the *K*-edge XMCD spectrum is not completely understood and further investigations are required.

The author expresses his thanks to the collaborators, M. Suzuki, M. Mizumaki (SPring-8), N. Kawamura, T. Ishikawa (RIKEN/SPring8), S. Uemura, S. Uemoto, H.Yamazaki, I. Harada (Okayama University), A. Koizumi, M. Takagaki, N. Sakai (Himeji Inst. Technology), D. Fruchart (CNRS, Grenoble), A. Kotani (ISSP, University of Tokyo), and T. Fijikawa (Chiba University). These studies were carried out under the approval of SPring-8 PRC (Proposal Nos. 1997B0154, 1998A0253, 1999A0173, 1999B0385, and 2000A0383).

References

Alagna, L., Prosperi, T., Turchini, S., Goulon, J., Rogalev, A., Goulon-Ginet, C., Natoli, C. R., Peacock, R. D. & Stewart, B. (1998). *Phys. Rev. Lett.* **80**, 4799–4802.
Fruchart, D. & Bertaut, E. F. (1978). *J. Phys. Soc. Jpn*, **44**, 781–791.
Giles, C., Malgrange, C., Goulon, J., de Bergevin, F., Vettier, C., Dartyge, E., Fontaine, A., Giorgetti, C. & Pizzini, S. (1994). *J. Appl. Cryst.* **27**, 232–240.
Goulon, J., Brookes, N. B., Gauthier, C., Goedkoop, J., Goulon-Ginet, C., Hagelstein, M. & Rogalev, A. (1995). *Physica B*, **208**&**209**, 232.
Harada, I. & Kotani, A. (1994). *J. Phys. Soc. Jpn*, **63**, 1285–1288.
Igarashi, J. & Hirai, K. (1994). *Phys. Rev. B*, **50**, 17820–17829.
Ishikawa, T., Hirano, K., Kanzaki, K. & Kikuta, S. (1992). *Rev. Sci. Instrum.* **63**, 1098–1103.
Kaneko, T., Kanomata, T. & Shirakawa, K. (1987). *J. Phys. Soc. Jpn*, **56**, 4047–4055.
Kawamura, N., Maruyama, H., Kobayashi, K., Inoue, I. & Yamazaki, H. (1997). *J. Phys. IV Fr.* **7**(C1), 269–270.
Koizumi, A., Takagaki, M., Suzuki, M., Kawamura, N. & Sakai, N. (2000). *Phys. Rev. B*, **61**, R14909–R14912.
Krisch, M. H., Sette, F., Bergmann, U., Masciovecchio, C., Verbeni, R., Goulon, J., Caliebe, W. & Kao, C. C. (1996). *Phys. Rev. B*, **54**, R12673–R12676.
Maruyama, H., Iwazumi, T., Kawata, H., Koizumi, A., Fujita, M., Sakurai, H., Itoh, F., Namikawa, K., Yamazaki, H. & Ando, M. (1991). *J. Phys. Soc. Jpn*, **60**, 1456–1459.
Maruyama, H., Suzuki, M., Kawamura, N., Ito, M., Arakawa, E., Kokubun, J., Hirano, K., Horie, K., Uemura, S., Hagiwara, K., Mizumaki, M., Goto, S., Kitamura, H., Namikawa, K. & Ishikawa, T. (1999). *J. Synchrotron Rad.* **6**, 1133–1137.
Nagamatsu, S., Kawabe, Y. & Fujikawa, T. (2000). Private communication.
Rogalev, A., Doulon, J., Benayoun, G., Elleaume, P., Chavanne, J., Penel, Ch. & van Vaerenbergh, P. (1999). *SPIE*, **3773**, 275–283.
Schütz, G., Wagner, W., Wilhelm, W., Keinle, P., Zeller, R., Frahm, R. & Materlik, G. (1987). *Phys. Rev. Lett.* **58**, 737–740.
Sumiya, H., Toda, N., Nishibayashi, Y. & Satoh, S. (1997). *J. Cryst. Growth*, **178**, 485–494.
Suzuki, M., Kawamura, N., Mizumaki, M., Urata, A., Maruyama, H., Goto, S. & Ishikawa, T. (1998). *Jpn J. Appl. Phys.* **37**, L1488–L1490.
Suzuki, M., Kawamura, N., Mizumaki, M., Urata, A., Maruyama, H., Goto, S. & Ishikawa, T. (1999). *J. Synchrotron Rad.* **6**, 190–192.
Uemoto, S., Maruyama, H., Kawamura, N., Uemura, S., Kitamoto, N., Nakao, H., Hara, S., Suzuki, M., Fruchart, D. & Yamazaki, H. (2001). *J. Synchrotron Rad.* **8**, 449–451.